Time-Domain Impedance Boundary Conditions for Computational Aeroacoustics

Christopher K. W. Tam* and Laurent Auriault†

Florida State University, Tallahassee, Florida 32306-3027

It is an accepted practice in aeroacoustics to characterize the properties of an acoustically treated surface by a quantity known as impedance. Impedance is a complex quantity. As such, it is designed primarily for frequency-domain analysis. Time-domain boundary conditions that are the equivalent of the frequency-domain impedance boundary condition are proposed. Both single frequency and model broadband time-domain impedance boundary conditions are provided. It is shown that the proposed boundary conditions, together with the linearized Euler equations, form well-posed initial boundary value problems. Unlike ill-posed problems, they are free from spurious instabilities that would render time-marching computational solutions impossible.

Nomenclature

a_0	= speed of sound
k	= total wave number
M	= Mach number
p	= pressure
R	= acoustic resistance
R_a	= artificial mesh Reynolds number
$Re(\ )$	= real part
t	= time
u, v, w	= velocity components
v	= velocity vector
v_n	= velocity component normal to impedance surface (positive pointing to the surface)
X	= acoustic reactance
Z	= impedance
α, β	= wave number components (Fourier transform variables)
Δt	= time step
Δx	= mesh size
ρ	= gas density
Ω, ω	= angular frequency

I. Introduction

NOWADAYS, acoustic treatment is invariably used on the inside surface of all commercial aircraft jet engines for fan noise reduction. Acoustic treatment panels, when properly tuned, are extremely effective noise suppressors.[1] Because of structural integrity requirements, the treatment panels are usually of the Helmholtz resonator type. The damping mechanism of these types of panels are generally attributed to the dissipation associated with the oscillatory jets formed at the mouths of the Helmholtz resonators[2-4] (see Fig. 1). These jets are induced by the pressure fluctuations accompanying the passage of acoustic disturbances over the surface of the treatment panels.

The flow and acoustic fields around the Helmholtz resonators of the treatment panels are exceedingly complicated, especially when there is a mean flow adjacent to the panel. Figure 2 shows schematically the oscillatory jets at the mouths of the Helmholtz oscillators or cavities induced by pressure waves in the presence of a mean flow as observed by Baumeister and Rice[3,4] in a water channel simulation.

For engineering purposes, a gross macroscopic description of the effects of the treatment panels on the incident acoustic waves is

definitely preferred over a more demanding microscopic description of the actual phenomenon. In the aeroacoustics community, it is an accepted practice to characterize the macroscopic properties of an acoustically treated surface by a single quantity Z called the impedance. The impedance is defined as the ratio of the acoustic pressure p to the acoustic velocity component normal to the treated surface v_n (positive when pointing into the surface). That is,

$$p = Zv_n \qquad (1)$$

Impedance is a complex quantity, $Z = R - iX$ ($e^{-i\omega t}$ dependence is assumed). The use of a complex quantity is needed to account for the damping and phase shift imparted on the sound waves by the acoustically treated surface. The acoustic resistance R and the acoustic reactance X are generally frequency dependent. They also vary with the intensity of the incident sound waves and the adjacent mean flow velocity. These quantities are usually measured empirically, although some semi-empirical formulas are available for their estimates, provided the construction of the panels is sufficiently simple. Figure 3 shows a typical set of measured resistance and reactance data for a 6.7%-perforate treatment panel at low sound intensity given in Ref. 1. An important feature is that R is positive and does not vary much with frequency. On the other hand, X can be both positive or negative depending on the frequency. The dependence of X on frequency can be represented by a simple analytical

Fig. 1 Schematic diagram of the oscillatory jets induced by incident acoustic waves at the mouths of the Helmholtz resonators of a treatment panel.
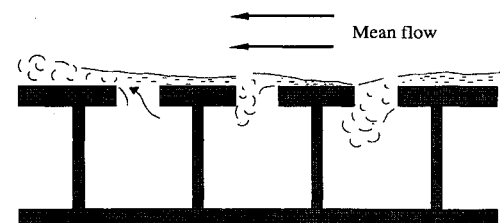
Fig. 2 Schematic diagram of the oscillatory jets induced by sound waves in the presence of a mean flow.
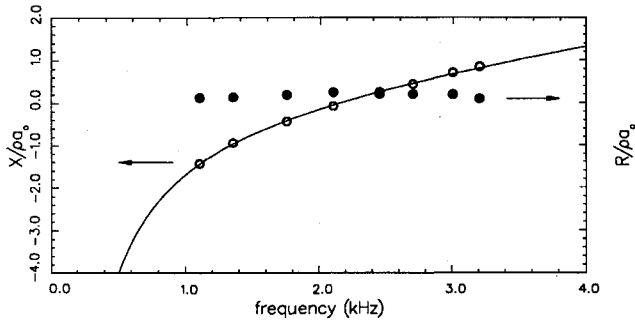
Fig. 3 Dependence of the resistance and reactance of a 6.7%-perforate treatment panel on frequency at low sound intensity (no flow) given in Ref. 1; o, reactance and •, resistance.

expression. For instance, the data in Fig. 3 are accurately represented by a two parameter formula,

$$X/\rho a_0 = (X_{-1}/\omega) + X_1\omega \tag{2}$$

The parameters X_{-1} and X_1 are found by mean-least-square fit to be -13.48 and 0.0739, respectively, where ω is measured in kilo-radian/second.

Impedance boundary condition (1) is basically a boundary condition established for frequency-domain analysis. As it is, it cannot be used in time-domain computation. The primary objective of this paper is to derive a suitable equivalent of the impedance boundary condition in the time domain. Such a boundary condition has not been considered before. Time-domain impedance boundary condition would allow the use of the newly developed computational aeroacoustics methods for the solution of duct acoustics and turbomachinery noise problems. One significant advantage of time-domain methods over frequency domain methods is that broadband noise problems can be handled relatively easily, almost without extra effort. For broadband noise problems, frequency domain methods are computationally intensive and laborious.

Time-domain problems can be solved only if they are well posed. One of the requirements of well-posedness is that the mathematical problem is stable and dependent continuously on the initial and boundary data. In this paper, it will be shown that the time-domain impedance boundary conditions developed do not lead to ill-posed mathematical problems. There are no spurious unstable solutions. Results of direct numerical simulations using these newly developed time-domain impedance boundary conditions are found to agree well with analytical solutions.

In the presence of a mean flow, the standard formulation of the impedance boundary condition[5] is known to give rise to a spurious unstable solution of the Kelvin–Helmholtz type.[6] A general proof of the existence of such instability is provided here. Because of this instability, time-domain methods cannot be successfully implemented. An alternative way of prescribing the impedance condition, that would not lead to an ill-posed initial boundary value problem, is proposed. A time-domain solution is possible when the proposed impedance boundary condition is used.

II. Single-Frequency Time-Domain Impedance Boundary Condition

A. Time-Domain Impedance Boundary Condition

Let us first consider the case in which the sound field consists of a single frequency Ω ($\Omega > 0$). That is, the pressure and velocity fields of the sound waves have time dependence, at $t \to \infty$, of the form $p(x, t) = Re[\hat{p}(x)e^{-i\Omega t}]$ and $v(x, t) = Re[\hat{v}(x)e^{-i\Omega t}]$. Suppose the resistance and reactance of a treatment panel at angular frequency Ω is R and X; then a suitable set of time-domain boundary condition at the surface of the panel is

$$X < 0, \qquad \frac{\partial p}{\partial t} = R\frac{\partial v_n}{\partial t} - X\Omega v_n \tag{3}$$

$$X \geq 0, \qquad p = Rv_n + \frac{X}{\Omega}\frac{\partial v_n}{\partial t} \tag{4}$$
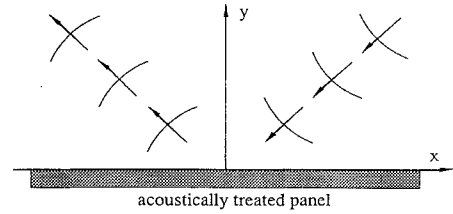

Fig. 4 Sound field adjacent to an acoustically treated panel.

It is easy to verify by direct substitution that Eq. (3) or (4) yields the frequency-domain impedance boundary condition $p = Zv_n (Z = R - iX)$ for a sound field of single frequency Ω. The reason why boundary condition (3) should not be used when X is positive is that it will lead to spurious unstable solutions. In other words, Eq. (3) will give rise to ill-posed initial boundary value problems for $X > 0$. The same reason applies to the restriction imposed on boundary condition (4).

B. Well-Posedness of Time-Domain Impedance Boundary Condition

To show that Eq. (3) or (4) leads to well-posed initial boundary value problems, we will consider a plane treatment panel adjacent to a sound field as illustrated in Fig. 4. For simplicity, we will let the surface of the panel be the x–z plane. In terms of dimensionless variables with L (a typical length of the problem) as the length scale, a_0 as the velocity scale, L/a_0 as the time scale, ρ_0 (the ambient gas density) as the density scale, and $\rho_0 a_0^2$ as the pressure scale, the acoustic field equations (the linearized momentum and energy equations) are

$$\frac{\partial v}{\partial t} = -\nabla p \tag{5}$$

$$\frac{\partial p}{\partial t} = -\nabla \cdot v \tag{6}$$

Let $\tilde{f}(\alpha, \beta, \omega)$ be the Fourier–Laplace transform of a function $f(x, z, t)$. The functions $\tilde{f}$ and f are related by

$$\tilde{f}(\alpha, \beta, \omega) = \frac{1}{(2\pi)^3} \int\int_{-\infty}^{\infty}\int_0^{\infty} f(x, z, t)$$
$$\times \exp[-i(\alpha x + \beta z - \omega t)]\, dt\, dx\, dz \tag{7}$$

$$f(x, z, t) = \int\int_{-\infty}^{\infty}\int_{\Gamma} \tilde{f}(\alpha, \beta, \omega)$$
$$\times \exp[i(\alpha x + \beta z - \omega t)]\, d\omega\, d\alpha\, d\beta \tag{8}$$

By applying Fourier–Laplace transforms to Eqs. (5) and (6), it is easy to find that the solution that satisfies radiation or outgoing wave condition at $y \to \infty$ is

$$\begin{bmatrix} \tilde{p} \\ \tilde{v} \end{bmatrix} = A \begin{bmatrix} 1 \\ (\hat{\omega}^2 - 1)^{\frac{1}{2}}/\hat{\omega} \end{bmatrix} \exp\left[ik(\hat{\omega}^2 - 1)^{\frac{1}{2}}y\right] \tag{9}$$

where $k = (\alpha^2 + \beta^2)^{1/2}$, $\hat{\omega} = \omega/k$ and v is the velocity component in the y direction (note that $v = -v_n$). The branch cuts of the function $(\hat{\omega}^2 - 1)^{1/2}$ are taken to be $0 \leq \arg(\hat{\omega}^2 - 1)^{1/2} \leq \pi$; the left (right) equality is to be used if $\hat{\omega}$ is real and positive (negative). The branch cut configuration in the $\hat{\omega}$ plane is shown in Fig. 5. The Fourier–Laplace transforms of boundary conditions (3) and (4) (in dimensionless form with $\rho_0 a_0$ as the scale of impedance) are

$$X < 0, \qquad \tilde{p} = [-R + (iX\Omega/k\hat{\omega})]\tilde{v} \tag{10}$$

$$X \geq 0, \qquad \tilde{p} = [-R + (i\hat{\omega}kX/\Omega)]\tilde{v} \tag{11}$$

Substitution of Eq. (9) into Eqs. (10) and (11) leads to the following dispersion relations:

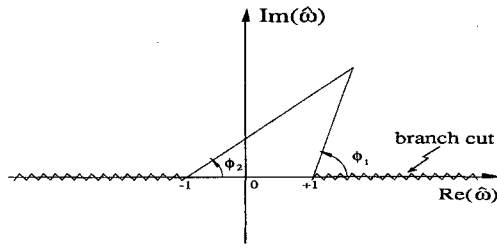$$X < 0, \qquad \frac{\hat{\omega}^2}{(\hat{\omega}^2 - 1)^{\frac{1}{2}}} + R\hat{\omega} = \frac{iX\Omega}{k} \tag{12}$$

Fig. 5   Branch cut configuration for $(\hat{\omega}^2 - 1)^{1/2}$. Argument of $(\hat{\omega}^2 - 1)^{1/2} = \frac{1}{2}(\phi_1 + \phi_2)$.
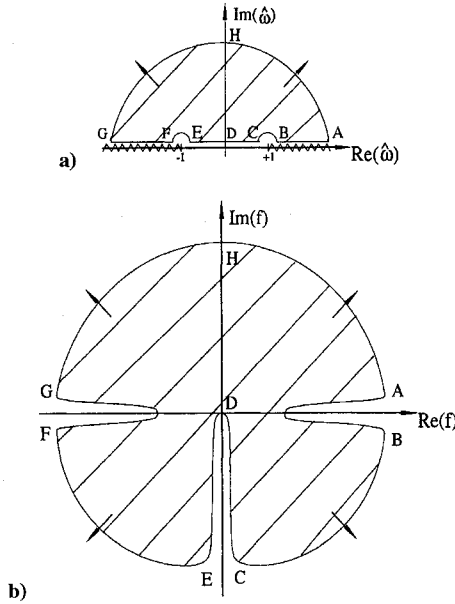

a)

b)

Fig. 6   Map of the upper half $\hat{\omega}$ plane in the f plane: a) $\hat{\omega}$ plane and b) f plane.

$$X \ge 0, \qquad \frac{\hat{\omega}}{(\hat{\omega}^2 - 1)^{\frac{1}{2}}} - i\frac{kX}{\Omega}\hat{\omega} = -R \qquad (13)$$

Initial boundary value problems involving governing equations (5) and (6) and boundary conditions (3) or (4) are stable and well posed if dispersion relations (12) and (13) have no solutions in the upper half $\hat{\omega}$ plane. To prove that this is the case, let the left-hand side of Eqs. (12) and (13) be denoted by $f(\hat{\omega})$ and $g(\hat{\omega})$, respectively:

$$f(\hat{\omega}) = \frac{\hat{\omega}^2}{(\hat{\omega}^2 - 1)^{\frac{1}{2}}} + R\hat{\omega} \qquad (14)$$

$$g(\hat{\omega}) = \frac{\hat{\omega}}{(\hat{\omega}^2 - 1)^{\frac{1}{2}}} - i\frac{kX}{\Omega}\hat{\omega} \qquad (15)$$

Figures 6 and 7 show the maps of the upper half $\hat{\omega}$ plane in the f and g planes. The shaded region represents the image points of the upper half $\hat{\omega}$ plane. Since the right-hand side of Eq. (12) is purely imaginary and negative, and the shaded region in the f plane does not include the negative imaginary axis, no value of $\hat{\omega}$ in the upper half $\hat{\omega}$ plane can satisfy dispersion relation (12). Also, the right-hand side of Eq. (13) is real and negative so that it will not lie in the shaded region of Fig. 7. Thus, dispersion relation (13) has no solution in the upper half $\hat{\omega}$ plane. Therefore, Eqs. (3) and (4) would lead to well-posed problems. On the other hand, it is easy to show if boundary condition (3) is used when X is positive or boundary condition (4) is used when X is negative, there will be unstable roots associated with dispersion relations (12) and (13). In these cases, there will be spurious unstable solutions and the initial boundary value problems are ill posed.
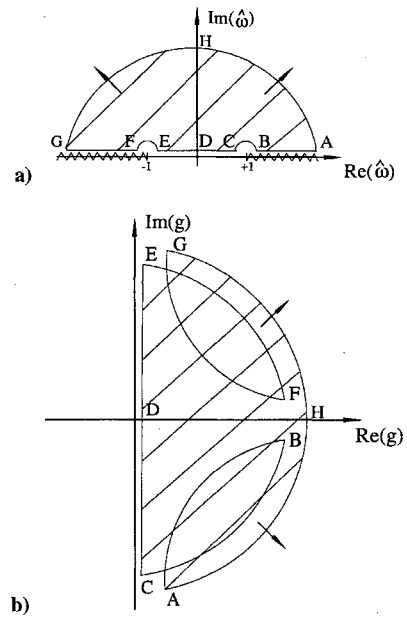

a)

b)

Fig. 7   Map of the upper half $\hat{\omega}$ plane in the g plane: a) $\hat{\omega}$ plane and b) g plane.
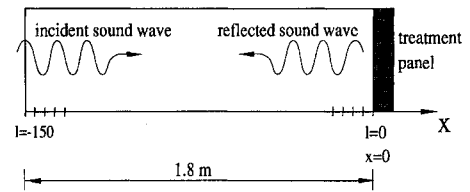

Fig. 8   Normal incidence impedance tube.

C.   Numerical Implementation and Results

To illustrate the effectiveness of time-domain impedance boundary conditions (3) and (4), we will apply them to the numerical simulation of the standing wave pattern of the normal-incidence impedance tube problem.[1,7-9] The impedance tube is designed to measure the impedance of an acoustic liner sample. The sample is placed at one end of a long tube as shown in Fig. 8. A single frequency acoustic wave train is introduced at the open end. The sound waves are reflected off the surface of the acoustically treated panel. The incident and reflected waves form a standing wave pattern. By measuring the standing wave ratio of the pressure envelope and the relative phase of the incident and reflected waves (from the position of the first minimum of the pressure envelope) the impedance of the treatment panel can be determined.[1,9]

Now let us consider an impedance tube of length 1.8 m. The speed of sound at room temperature is 340 m/s. To ensure there are at least seven mesh points per wavelength in the computation for sound frequency up to 4 kHz, we will divide the impedance tube into 150 mesh spacings yielding $\Delta x = 0.012$ m. In the rest of this paper, Δx is used as the length scale in all of the computations (i.e., $L = \Delta x$). We will assume that the treatment panel is the 6.7% perforate of Fig. 3. The equations governing the acoustic field inside the tube are the one-dimensional version of Eqs. (5) and (6). They are

$$\frac{\partial}{\partial t}\begin{bmatrix} u \\ p \end{bmatrix} = -\frac{\partial}{\partial x}\begin{bmatrix} p \\ u \end{bmatrix} \qquad (16)$$

The time-domain boundary condition to be applied at $x = 0$, the right end of the tube, is

$$X < 0, \qquad \frac{\partial p}{\partial t} = R\frac{\partial u}{\partial t} - X\Omega u \qquad (17a)$$

$$X \ge 0, \qquad p = Ru + \frac{X}{\Omega}\frac{\partial u}{\partial t} \qquad (17b)$$

The incident sound wave will be taken to be

$$p_{\text{incident}} = u_{\text{incident}} = \cos[\Omega(x - t)]$$

At the left end of the tube, the radiation boundary condition is to be enforced. Such radiation boundary condition has been formulated by Tam.[10] It may be written in the form

$$\frac{\partial}{\partial t}\begin{bmatrix} u \\ p \end{bmatrix} = \frac{\partial}{\partial x}\begin{bmatrix} u \\ p \end{bmatrix} + \begin{bmatrix} 1 \\ 1 \end{bmatrix} 2\Omega \sin[\Omega(x - t)] \qquad (18)$$

The nonhomogeneous term in Eq. (18) is from the incident acoustic waves.

We will use the seven-point stencil dispersion-relation-preserving (DRP) time-marching scheme[10,11] for the numerical solution of the impedance tube problem. The DRP scheme was designed for high-quality numerical solution of aeroacoustics problems. It is highly accurate even when as few as seven mesh points per wavelength are used in the computation. The discretized form of the right-hand side of Eq. (16) is

$$K_\ell^{(n)} = -\sum_{j=-3}^{3} a_j p_{\ell+j}^{(n)} - \frac{1}{R_a} \sum_{j=-3}^{3} d_j u_{\ell+j}^{(n)} \qquad (19)$$

$$L_\ell^{(n)} = -\sum_{j=-3}^{3} a_j u_{\ell+j}^{(n)} - \frac{1}{R_a} \sum_{j=-3}^{3} d_j p_{\ell+j}^{(n)} \qquad (20)$$

where subscript ℓ is the spatial index; $\ell = 0, -1, -2, \ldots, -150$, and superscript n denotes the time level. The coefficients a_j and d_j are provided in Ref. 10. The last terms on the right-hand sides of Eqs. (19) and (20) are the artificial selective damping terms.[12] The artificial selective damping terms are designed to remove any spurious short wavelength numerical waves inside the computation domain. It can be shown that the damping terms do not affect the part of the solution that has wavelength longer than seven mesh spacings. In the present computation, $R_a = 20$ has been used.

The impedance boundary condition (3) or (4) or (17) is to be imposed at $\ell = 0$. Here, we will follow Ref. 13 and introduce a ghost value of pressure p_1 at $\ell = 1$. The ghost value p_1 is to be chosen so that both the governing equation (16) and the impedance boundary condition are satisfied at the boundary point $\ell = 0$. The addition of a ghost value at $\ell = 1$ allows Eq. (19) to be applied to $-147 \leq \ell \leq -2$, whereas Eq. (20) is used only for $-147 \leq \ell \leq -3$.

To march in time, the DRP scheme uses the following four-time-level algorithm:

$$\begin{bmatrix} u \\ p \end{bmatrix}_\ell^{(n+1)} = \begin{bmatrix} u \\ p \end{bmatrix}_\ell^{(n)} + \Delta t \sum_{j=0}^{3} b_j \begin{bmatrix} K \\ L \end{bmatrix}_\ell^{(n-j)} \qquad (21)$$

Coefficients b_j may be found in Ref. 10. This time-marching algorithm applies to all points on the computation grid; $\ell = 0, -1, -2, \ldots, -150$. For the last three points on the left-hand side of the computation domain; i.e., $\ell = -150, -149, -148$, $K_\ell^{(n)}$ and $L_\ell^{(n)}$ are obtained by applying backward difference to the spatial derivative terms on the right-hand side of radiation boundary condition (18). Similarly, for the boundary points on the right end of the tube, the expressions for $K_\ell^{(n)}$ and $L_\ell^{(n)}$ are obtained by backward differencing the right-hand side of (16). Artificial selective damping terms similar to that of Eq. (19), but with reduced stencil size,[10] are again added.

To enforce the impedance boundary condition (3) or (4) or (17) at $\ell = 0$, we note that $\partial p/\partial t$ and $\partial u/\partial t$ are given by Eq. (16). On eliminating the time derivative terms by Eq. (16), the impedance boundary condition at $\ell = 0$ becomes

$$X < 0, \qquad \frac{\partial u}{\partial x} = R\frac{\partial p}{\partial x} + \Omega X u \qquad (22)$$

$$X \geq 0, \qquad p = Ru - \frac{X}{\Omega}\frac{\partial p}{\partial x} \qquad (23)$$

upon discretizing Eq. (22) or (23), at time level $(n+1)$ by backward differences, an algebraic equation involving the ghost value $p_1^{(n+1)}$
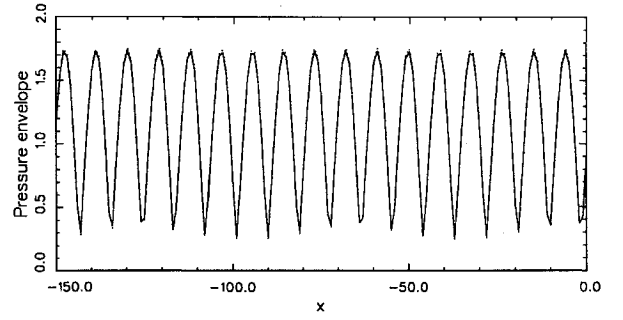

Fig. 9 Spatial distribution of the pressure envelope in a normal-incidence impedance tube at 1600 Hz frequency: ——, time-domain solution (DRP scheme) and · · · ·, exact (frequency-domain) solution.
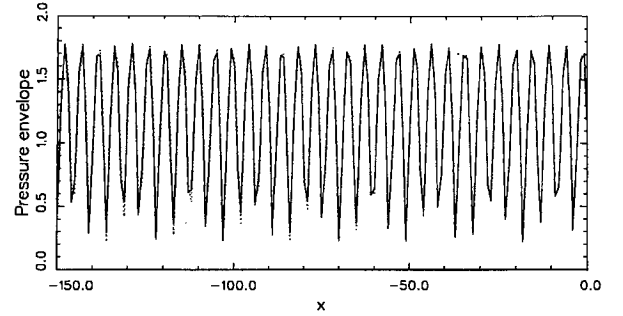

Fig. 10 Spatial distribution of the pressure envelope in a normal-incidence impedance tube at 3000 Hz frequency: ——, time-domain solution (DRP scheme) and · · · ·, exact (frequency-domain) solution.

is obtained. This equation provides the formula by which the ghost value may be found. For instance, if Eq. (22) is used, we find

$$p_1^{(n+1)} = \frac{1}{Ra_1^{51}}\left(\sum_{j=-6}^{0} a_j^{60} u_{j+0}^{(n+1)} - \Omega X u_0^{(n+1)} - R\sum_{j=-5}^{0} a_j^{51} p_j^{(n+1)} \right) \qquad (24)$$

In carrying out the time-marching DRP algorithm, the computation follows the following procedure. After the solution at time level n has been found, the values of u and p are updated to the next time level $(n+1)$ by Eq. (21) at every point on the grid except the ghost point. The ghost value $p_1^{(n+1)}$ is calculated by Eq. (24). With the ghost value found, the calculation proceeds to the next time level $(n+2)$. The entire process is then repeated.

Figure 9 shows a comparison of the time-domain solution of the pressure envelope along the full length of the impedance tube calculated by the DRP scheme and the exact frequency-domain solution at a frequency of 1.6 kHz. At this frequency X is negative so that impedance boundary condition (3) was used in the numerical solution. Figure 10 shows a similar comparison at a frequency of 3.0 kHz. In this case X is positive. Accordingly, impedance boundary condition (4) was employed. The time-domain solutions compare well with the exact frequency-domain results. The peak values and their locations, which are important quantities in impedance tube experiments, are accurately calculated. These simulations suggest that time-domain solutions involving impedance boundaries are feasible and accurate. Moreover, the proposed time-domain impedance boundary condition, indeed, leads to well-posed initial boundary value problems.

III. Broadband Time-Domain Impedance Boundary Condition

A. Three-Parameter Broadband Model

Both the resistance and impedance of an acoustic treatment panel of the Helmholtz resonator type are frequency dependent. Figure 3 shows measured data typical of such panels, as reported in Ref. 1. It is seen that over the frequency range of interest, 1–3 kHz, the variation in the resistance is small. However, there is a significant

change in the reactance. The measured data of Fig. 3 can be closely approximated by analytical formulas of the form

$$R = R_0, \qquad X = (X_{-1}/\omega) + X_1\omega \tag{25}$$

where $R_0(R_0 > 0)$, $X_{-1}(X_{-1} < 0)$, and $X_1(X_1 > 0)$ are parameters. The values of these parameters are determined by mean-least-square fit to the data. The impedance corresponding to this three-parameter model is

$$Z = R_0 - i[(X_{-1}/\omega) + X_1\omega] \tag{26}$$

Now we propose the use of the following time-domain impedance boundary condition:

$$\frac{\partial p}{\partial t} = R_0 \frac{\partial v_n}{\partial t} - X_{-1}v_n + X_1 \frac{\partial^2 v_n}{\partial t^2} \tag{27}$$

It is straightforward to show by assuming time dependence of the form $e^{-i\omega t}$ that Eq. (27) is equivalent to the frequency-domain impedance boundary condition with the impedance given by Eq. (26). But before Eq. (27) is applied to any large-scale computation, it is prudent to show that this boundary condition would not give rise to spurious instabilities.

B. Stability of Three-Parameter Time-Domain Impedance Boundary Condition

Let us return to the boundary value problem of Fig. 4. It will be assumed that the time-domain impedance boundary condition (27) is to be imposed at the x–z plane. The Fourier–Laplace transform of Eq. (27) is

$$-\omega\tilde{p} = \left[-\omega R_0 + i\left(X_{-1} + \omega^2 X_1\right)\right]\tilde{v}_n \tag{28}$$

Substitution of Eq. (9) into Eq. (28) results in the dispersion relation

$$\frac{\omega^2}{(\omega^2 - k^2)^{\frac{1}{2}}} + \omega R_0 - iX_1\omega^2 = iX_{-1} \tag{29}$$

where the branch cuts of the function $(\omega^2 - k^2)^{1/2}$ are to be taken such that $0 \le \arg(\omega^2 - k^2)^{1/2} \le \pi$; the left (right) equality is to be used if ω is real and positive (negative). Let

$$F(\omega) = \frac{\omega^2}{(\omega^2 - k^2)^{\frac{1}{2}}} + \omega R_0 - iX_1\omega^2 \tag{30}$$

that is, the left-hand side of Eq. (29). By tracing over the contour $ABCDEFGH$ in the upper half ω plane, it is easy to establish that the upper half ω plane is mapped into the shaded region in the F plane as shown in Fig. 11. The mapped region does not include the negative imaginary axis. Now X_{-1}, on the right-hand side of Eq. (29), is negative. This means that no value of ω in the upper half ω plane would satisfy dispersion relation (29). Thus, the solutions of the initial boundary value problems are stable.

C. Numerical Implementation and Comparison with Exact Solution

We will consider an initial value problem associated with the normal-incidence impedance tube (see Fig. 8) to illustrate how the time-domain impedance boundary condition (27) can be implemented. With respect to a fixed point in space, a transient acoustic pulse produces a broadband pressure field in the frequency domain. Thus, for a time-dependent acoustic pulse problem, the broadband impedance boundary condition should be used at the right terminal of the tube.

Equation (16) is the governing equation of the problem. Now, at the impedance surface, $\ell = 0$, boundary condition (27) may be rewritten in the following form after eliminating $\partial p/\partial t$ by the second equation of (16):

$$\frac{d^2u_0}{dt^2} = \frac{1}{X_1}\left[-\left(\frac{\partial u}{\partial x}\right)_0 - R_0\frac{du_0}{dt} + X_{-1}u_0\right] \tag{31}$$

We will rewrite this equation as a first-order system in time. Let
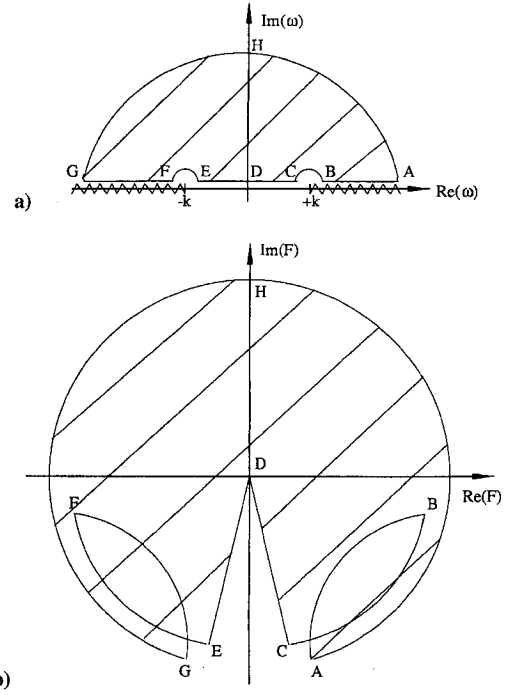
$$v_0 = \frac{du_0}{dt} \tag{32}$$

Fig. 11 Map of the upper half ω plane in the F plane: a) ω plane and b) F plane.

Equation (31) may be casted into the following system of equations:

$$\frac{d}{dt}\begin{bmatrix} u_0 \\ v_0 \end{bmatrix} = \begin{bmatrix} v_0 \\ \frac{1}{X_1}\left(-\sum_{j=-6}^{0} a_j^{60}u_j - R_0v_0 + X_{-1}u_0\right) \end{bmatrix} \tag{33}$$

In Eq. (33) the term $(\partial u/\partial x)_0$ has been replaced by a seven-point backward difference according to the DRP scheme. Upon discretizing Eq. (33) in time, we find

$$\begin{bmatrix} u_0 \\ v_0 \end{bmatrix}^{(n+1)} = \begin{bmatrix} u_0 \\ v_0 \end{bmatrix}^{(n)}$$

$$+ \Delta t \sum_{j=0}^{3} b_j \left[\frac{1}{X_1}\left(-\sum_{j=-6}^{0} a_j^{60}u_j - R_0v_0 + X_{-1}u_0\right) \right]^{(n-j)} \tag{34}$$

But the value $u_0^{(n+1)}$ can also be found from the discretized form of governing equation (16), namely, Eq. (21). The value $u_0^{(n+1)}$ calculated by either Eq. (21) or Eq. (34) must be the same. This provides the condition for determining the ghost value $p_1^{(n)}$. The explicit expression for $p_1^{(n)}$ is

$$p_1^{(n)} = \frac{1}{b_0 a_1^{51}\Delta t}\left(-u_0^{(n+1)} + u_0^{(n)}\right.$$

$$\left. + \Delta t \sum_{j=1}^{3} b_j K_0^{(n-j)} - \Delta t b_0 \sum_{j=-5}^{0} a_j^{51} p_j^{(n)}\right) \tag{35}$$

The boundary condition on the left end of the tube is still given by Eq. (18) except that the nonhomogeneous terms should be omitted as there is no incoming wave.

We will assume that the disturbance is generated by the following initial conditions at $t = 0$:

$$u = 0, \qquad p = \exp[-0.0044(x + 83.333)^2]\cos[0.444(x + 83.333)] \tag{36}$$
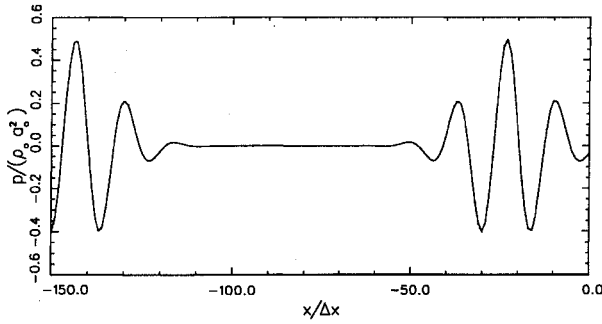
Fig. 12 Pressure waveform of the incident acoustic pulse inside the normal-incidence impedance tube at $t = 60.1$: ——, time-domain solution (DRP scheme) and · · · ·, exact solution.
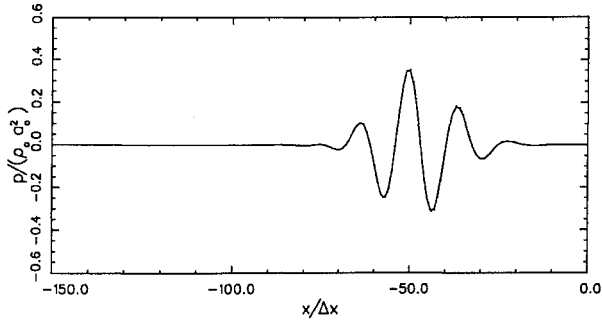

Fig. 13 Pressure waveform of the reflected acoustic pulse inside the normal-incidence impedance tube at $t = 140.1$: ——, time-domain solution (DRP scheme) and · · · ·, exact solution.

Here, the same dimensionless variables as in Sec. II.C are used. This choice of initial conditions ensures that the center of the acoustic spectrum of the incident wave at the surface of the acoustic treatment panel has a frequency of 2 kHz and a spectrum half-width of 0.5 kHz. In this example, the values of the dimensionless parameters of Eq. (27) are obtained by fitting Eq. (25) to the data of Fig. 3.

Figure 12 shows the computed pressure distribution at time $t = 60.1$. At this time, the left half of the initial pulse is about to exit the computation domain, whereas the right half of the pulse is about to impinge on the surface of the treatment panel. The dotted curve is the exact solution. Figure 13 shows the reflected pulse propagating away from the impedance boundary of the tube at $t = 140.1$. The amplitude of the reflected pulse is considerably smaller than that of the incident pulse. Part of the acoustic energy is dissipated during the reflection process off the impedance surface. The exact frequency-domain solution is represented by the dotted curve. There is excellent agreement between numerical results and the exact solution. This is true in both the wave amplitude and phase. This example provides further confidence in the use of time-domain impedance boundary conditions.

IV. Impedance Boundary Condition in the Presence of a Subsonic Mean Flow

A. Traditional Model

In jet engines, the acoustic treatment panel is always placed next to a mean flow. Traditionally,[5] the impedance boundary condition in the presence of a mean flow is formulated with the assumption of the existence of a very thin zero-velocity fluid layer at the surface of the treatment panel. At the interface of the zero-velocity fluid layer and the mean flow, the condition of continuity of particle displacement is used. In dimensionless variables, the frequency-domain impedance boundary condition, after simplification, may be written as

$$-i\omega p + M\frac{\partial p}{\partial x} = -i\omega Z v_n \qquad (37)$$

where M is the mean flow Mach number, and x is in the direction of the mean flow.

In an extensive numerical study of the normal modes of a duct with treatment panels, Tester[6] found that boundary condition (37)
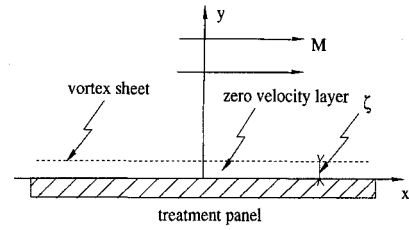

Fig. 14 Schematic diagram showing a postulated zero-velocity layer adjacent to an acoustically treated panel in the presence of a mean flow.

led to an unstable solution. The unstable solution is of the Kelvin–Helmholtz type arising from the vortex sheet interface between the mean flow and the zero-velocity fluid layer. In standard duct acoustics analysis using frequency-domain approach, this instability is either not mentioned or totally ignored.[5] We will now show that the use of boundary condition (37) always gives rise to an unstable solution.

The linearized momentum and energy equations governing the sound field superimposed on a uniform mean flow of Mach number M in the x direction (see Fig. 14) are

$$\frac{\partial v}{\partial t} + M\frac{\partial v}{\partial x} = -\nabla p \qquad (38)$$

$$\frac{\partial p}{\partial t} + M\frac{\partial p}{\partial x} + \nabla \cdot v = 0 \qquad (39)$$

By applying the Fourier–Laplace transform to Eqs. (38) and (39), it is easy to find that the solution that satisfies the outgoing wave condition at $y \to \infty$ is

$$\begin{bmatrix} \tilde{u} \\ \tilde{v} \\ \tilde{w} \\ \tilde{p} \end{bmatrix} = A \begin{bmatrix} \alpha/\tilde{\omega} \\ k(\hat{\omega}^2 - 1)^{\frac{1}{2}}/\tilde{\omega} \\ \beta/\tilde{\omega} \\ 1 \end{bmatrix} \exp\left[ik(\hat{\omega}^2 - 1)^{\frac{1}{2}}y\right] \qquad (40)$$

where $\tilde{\omega} = \omega - M\alpha$, $k = (\alpha^2 + \beta^2)^{1/2}$, and $\hat{\omega} = \tilde{\omega}/k$. The branch cuts of the function $(\hat{\omega}^2 - 1)^{1/2}$ are the same as those stipulated just after Eq. (9).

Substitution of Eq. (40) into the Fourier–Laplace transform of boundary condition (37) yields the following dispersion relation:

$$\frac{\hat{\omega}^2}{(\hat{\omega}^2 - 1)^{\frac{1}{2}}} + Z\hat{\omega} = -\frac{\alpha}{k}MZ \qquad (41)$$

Now let the left-hand side of Eq. (41) be denoted by $\bar{f}(\hat{\omega})$:

$$\bar{f}(\hat{\omega}) = \frac{\hat{\omega}^2}{(\hat{\omega}^2 - 1)^{\frac{1}{2}}} + Z\hat{\omega} \qquad (42)$$

Figure 15 shows the map of the upper half $\hat{\omega}$ plane in the $\bar{f}$ plane (shaded region) for $X > 0$. Since α can be positive or negative, there will always be values of α for which the point representing the right side of Eq. (41) lies in the shaded region of the $\bar{f}$ plane. Therefore, there will always be an unstable solution. If X is negative, a similar mapping procedure will show that there is always an unstable solution.

The existence of a Kelvin–Helmholtz-type instability renders the boundary value problem ill posed for the time-domain solution. The instability is, however, nonphysical. As pointed out before, its origin is in the postulate of a vortex sheet discontinuity right next to the impedance boundary. In reality, no such vortex sheet exists in the flow. It is an exaggerated idealization of a zero-thickness boundary layer. The pertinent point to remember is that the concept of impedance is just a gross macroscopic description of the effect of a treatment panel on the sound field. One could include the effect of the mean flow in the definition of the impedance directly without having to introduce its effect through the kinematic property of the vortex sheet discontinuity. If this is done, there is no need to assume the existence of a vortex sheet interface. A well-posed time-domain impedance boundary condition may then be derived. This possibility is discussed in the next subsection.
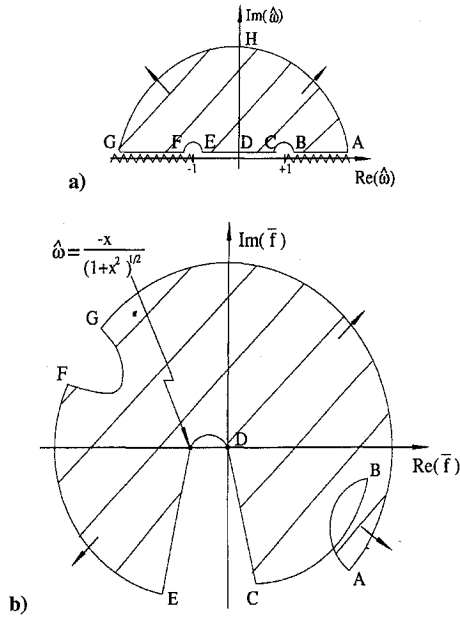
Fig. 15 Map of the upper half $\hat{\omega}$ plane in the $\bar{f}$ plane ($X > 0$): a) $\hat{\omega}$ plane and b) $\bar{f}$ plane.

B. Direct Interaction Model

The experimental studies of Baumeister and Rice[3,4] indicate that, for Helmholtz resonator type treatment panels, the jet flows at the mouths of the resonators or cavities interact directly with the mean flow outside. This is illustrated in Fig. 2. There is no zero-velocity fluid layer nor any vortex sheet discontinuity. When the boundary layer over the treatment panel is, indeed, thin, the jet flows at the mouths of the cavities are directly coupled to the mean flow. When this is the case, it would be more desirable not to introduce the mean flow effect through the kinematic condition of a vortex sheet discontinuity, but consider a direct interaction model by lumping the mean flow effects on the definition of impedance. What this amounts to is to define the impedance in exactly the same form as Eq. (1) even in the presence of a mean flow; i.e.,

$$p = Zv_n \tag{43}$$

where $Z = R - iX$ is the impedance. Here Z is a function of the mean flow. That is, R and X are flow Mach number dependent. Equation (43) is to replace Eq. (37). The relationship between R, X, and the mean flow Mach number must be found experimentally at this time. Further theoretical and experimental validation of this suggestion would certainly be useful and needed.

It is easy to show by the mapping technique that the dispersion relation arising from Eqs. (38) and (39) and boundary condition (43) does not give rise to an unstable solution. In other words, they form well-posed initial boundary value problems.

C. Single-Frequency and Three-Parameter Broadband Time-Domain Impedance Boundary Condition

If impedance boundary condition (43) is accepted instead of (37), then the single-frequency time-domain impedance boundary condition discussed in Sec. II and the three-parameter broadband model impedance boundary condition (27) can again be used. Specifically, for sound waves of a single frequency Ω, we have the time-domain impedance boundary condition

$$X < 0, \qquad \frac{\partial p}{\partial t} = R \frac{\partial v_n}{\partial t} - X\Omega v_n \tag{44}$$

$$X \geq 0, \qquad p = Rv_n + \frac{X}{\Omega} \frac{\partial v_n}{\partial t} \tag{45}$$

It can be easily shown that solutions of governing equations (38) and (39) and boundary condition (44) or (45) are stable. The same is true with boundary condition (27). That is, by omitting the fictitious vortex sheet discontinuity that is postulated in the traditional formulation of the impedance boundary condition, the resulting initial boundary value problems are well-posed and hence can be solved by time-domain methods.

V. Concluding Remarks

For Helmholtz resonator type of acoustic treatment panels, impedance is merely a macroscopic representation of the aggregated effects of the numerous microscopic cavity flows that take place in the surface region of the panel. In the presence of a mean flow, the actual flowfield in this region is extremely complicated. So far, it appears that no experiment has been performed to provide an adequate understanding of the microscopic cavity flowfields and their cumulative effects. This is, perhaps, not too surprising, for it is very difficult to make accurate time-dependent measurements in the small confined space of the cavities. Without such knowledge of the flowfield, the impedance of a panel can only be found empirically.

Recently, computational aeroacoustics methods have made impressive advances. It seems, therefore, that a feasible alternative to study the microscopic cavity flowfields is to use direct numerical simulations. Such simulations, when properly carried out, could shed light on the physical processes that lead to the damping and phase shifting of the acoustic wave field adjacent to the panel surface. When perfected, such time-domain simulations might even offer a way to determine the resistance and reactance of acoustic treatment panels from first principles.

Acknowledgment

References

[1]Motsinger, R. E., and Kraft, R. E., "Design and Performance of Duct Acoustic Treatment," *Aeroacoustics of Flight Vehicles: Theory and Practice*, NASA RP-1258, Aug. 1991, Chap. 14.

[2]Groeneweg, J. F., "Current Understanding of Helmholtz Resonator Arrays as Duct Boundary Conditions," *Basic Aerodynamic Noise Research*, NASA SP-207, July 1969, pp. 357–368.

[3]Baumeister, K. J., and Rice, E. J., "Visual Study of the Effect of Grazing Flow on the Oscillatory Flow in a Resonator Orifice," NASA TM X-3288, Sept. 1975.

[4]Baumeister, K. J., and Rice, E. J., "Flow Visualization in Long Neck Helmholtz Resonators with Grazing Flow," NASA TM X-73400, July 1976.

[5]Eversman, W. E., "Theoretical Models for Duct Acoustic Propagation and Radiation," *Aeroacoustics of Flight Vehicles: Theory and Practice*, NASA RP-1258, Aug. 1991, Chap. 13.

[6]Tester, B. J., "The Propagation and Attenuation of Sound in Lined Ducts Containing Uniform or Plug Flow," *Journal of Sound and Vibration*, Vol. 28, No. 2, 1973, pp. 151–203.

[7]Zorumski, W. E., and Tester, B.J., "Prediction of the Acoustic Impedance of Duct Liners," NASA TM X-73951, Sept. 1976.

[8]Lippert, W. K. R., "The Practical Representation of Standing Waves in an Acoustic Impedance Tube," *Acoustica*, Vol. 3, No. 3, 1953, pp. 153–160.

[9]Melling, T. H., "An Impedance Tube for Precision Measurement of Acoustic Impedance and Insertion Loss at High Sound Pressure Level," *Journal of Sound and Vibration*, Vol. 28, No. 1, 1973, pp. 23–54.

[10]Tam, C. K. W., "Computational Aeroacoustics: Issues and Methods," *AIAA Journal*, Vol. 33, No. 10, 1995, pp. 1788–1796.

[11]Tam, C. K. W., and Webb, J. C., "Dispersion-Relation-Preserving Finite Difference Schemes for Computational Acoustics," *Journal of Computational Physics*, Vol. 107, Aug. 1993, pp. 262–281.

[12]Tam, C. K. W., Webb, J. C., and Dong, Z., "A Study of the Short Wave Components in Computational Acoustics," *Journal of Computational Acoustics*, Vol. 1, March 1993, pp. 1–30.

[13]Tam, C. K. W., and Dong, Z., "Wall Boundary Conditions for High-Order Finite Difference Schemes in Computational Aeroacoustics," *Theoretical and Computational Fluid Dynamics*, Vol. 6, Oct. 1994, pp. 303–322.